A&A 506, 203–211 (2009)
DOI: 10.1051/0004-6361/200911871

The CoRoT space mission: early results

Astronomy & Astrophysics
Special feature

Improved fundamental parameters and LTE abundances of the CoRoT⋆ solar-type pulsator HD 49933⋆⋆

T. Ryabchikova[1,2], L. Fossati[1], and D. Shulyak[1]

[1] Institut für Astronomie, Universität Wien, Türkenschanzstrasse 17, 1180 Wien, Austria
e-mail: [ryabchik;fossati]@astro.univie.ac.at;denis.shulyak@gmail.com
[2] Institute of Astronomy, Russian Academy of Sciences, Pyatnitskaya 48, 119017 Moscow, Russia
e-mail: ryabchik@inasan.ru

Received 18 February 2009 / Accepted 7 May 2009

ABSTRACT

Aims. The knowledge of accurate stellar parameters is a key stone in several fields of stellar astrophysics, such as asteroseismology and stellar evolution. Although the parameters can be derived both from spectroscopy and multicolour photometry, the results obtained are sometimes affected by systematic uncertainties. In this paper, we present a self-consistent spectral analysis of the solar-type star HD 49933, which is a primary target for the CoRoT satellite.
Methods. We used high-resolution and high signal-to-noise ratio spectra to carry out a consistent parameter estimation abundance analysis of HD 49933. The LLMODELS code was employed for model atmosphere calculations, while SYNTH3 and WIDTH9 codes were used for line profile calculation and LTE abundance analysis.
Results. We provide a detailed description of the methodology adopted to derive the fundamental parameters and the abundances. Although the parameters obtained differ from the ones previously derived by other authors, we show that only the set obtained in this work is able to fit the observed spectrum accurately. In particular, the surface gravity was adjusted to fit pressure-sensitive spectral features.
Conclusions. We confirm the importance of a consistent analysis of relevant spectroscopic features, application of advanced model atmospheres, and the use of up-to-date atomic line data for the determination of stellar parameters. These results are crucial for further studies, e.g., detailed theoretical modelling of the observed pulsation frequencies.

Key words. stars: abundances – stars: fundamental parameters – stars: individual: HD 49933

1. Introduction

Several space missions have been launched to obtain high quality photometric data (e.g., WIRE, MOST, CoRoT) and several others are going to be launched in the near future (e.g., KEPLER, BRITE). One of the main goals of these missions is to provide astronomers with high precision photometric data that will allow a better understanding of stellar pulsation – the only approach that can improve our knowledge about stellar interiors.

The modelling of pulsational signals requires the knowledge of stellar parameters and primarily accurate values of the effective temperature ($T_{\rm eff}$) and metallicity (Z). The determination of fundamental parameters can be performed by different methods (some examples for stars from B- to G-type are: Fuhrmann et al. 1997; Przybilla et al. 2006; Fossati et al. 2009) that do not always lead to consistent results. Thus, it is important to choose a methodology that allows us to constrain the parameters of the star from the available observables (usually photometry and spectroscopy) in the most robust and reliable way.

After Mosser et al. (2005) discovered the presence of solar-like oscillations in HD 49933 using RV measurements from high resolution time-series spectra, this star was included as a primary CoRoT target for the photometric observation of solar-like oscillations. It was one of the first main sequence solar-type star in which solar-like oscillations were clearly detected from space photometry, due to the high quality data provided by the CoRoT satellite (Appourchaux et al. 2008).

Fundamental parameters and abundances of HD 49933 were obtained previously by different authors with different methods. The published fundamental parameters of HD 49933 display some scatter both in $T_{\rm eff}$ and $\log g$ (e.g., Edvardsson et al. 1993; Blackwell & Lynas-Gray 1998; Gillon & Magain 2006; Cenarro et al. 2007; Bruntt et al. 2008). As a consequence, the published abundances show some scatter. At the same time, a need for higher precision in stellar parameters for HD 49933 was emphasised by asteroseismic modelling of this object (Appourchaux et al. 2008; Kallinger et al. 2008), which employed new pulsation analysis techniques (e.g. Gruberbauer et al. 2008).

The main goal of the present work is to perform a consistent atmospheric and abundance analysis of HD 49933 that reproduces all of its photometric and spectroscopic data and investigate the degree to which the derived fundamental parameters depend on the applied methods.

⋆ The CoRoT space mission was developed and is operated by the French space agency CNES, with participation of ESA's RSSD and Science Programmes, Austria, Belgium, Brazil, Germany, and Spain.
⋆⋆ Figures 4, 5 and Tables 3, 4 are only available in electronic form at http://www.aanda.org

2. Observations and spectral reduction

Ten spectra of HD 49933 were obtained between 11 February 2006 and 13 February 2006 with the cross-dispersed echelle spectrograph HARPS (spectral resolution $R \sim 115\,000$) attached to the 3.6-m ESO La Silla telescope. The spectra were reduced with the online pipeline[1].

Each spectrum was obtained with an exposure time between 243 and 300 s. We retrieved the spectra from the ESO archive and co-added them to obtain a single spectrum with a signal-to-noise ratio (SNR) per pixel of about 500, calculated at ~5000 Å. The final spectrum, normalised by fitting a low order spline to carefully selected continuum points, covers the wavelength range 3780–6910 Å. The spectrum has a gap between 5300 Å and 5330 Å, since one echelle order is lost in the gap between the two chips of the CCD mosaic detector.

Figure 4 (online material) shows (from top to bottom) a sample of the first spectrum obtained on 11 February 2006, the last obtained on 13 February 2006 and the final co-added spectrum, around the strong Fe II line at 5018 Å.

3. The model atmosphere

To compute model atmospheres of HD 49933, we employed the LLMODELS stellar model atmosphere code (Shulyak et al. 2004). For all the calculations, Local Thermodynamical Equilibrium (LTE) and plane-parallel geometry were assumed. We used the VALD database (Piskunov et al. 1995; Kupka et al. 1999; Ryabchikova et al. 1999) as a source of atomic line parameters for opacity calculations. For a given model atmosphere, we performed a line selection procedure allowing us to choose lines that contribute significantly to the opacity for a given set of model parameters, adopting the selection threshold $\ell_\nu/\alpha_\nu \geqslant 1\%$, where α_ν and ℓ_ν are the continuum and line absorption coefficients at a given frequency ν. Convection was implemented according to the Canuto & Mazzitelli (1991a,b) model of convection (see Heiter et al. 2002, for more details).

4. Fundamental parameters and abundance analysis

Gillon & Magain (2006) used Strömgren indices to determine the atmospheric parameters of HD 49933. By using the TEMPLOGG code (Rogers 1995), they found that $T_{\rm eff} = 6543 \pm 200$ K, $\log g = 4.24 \pm 0.20$, and [Fe/H] $= -0.38 \pm 0.20$ dex. Although the uncertainties are quite large, we used this as our starting point in an iterative process in which we gradually improved the parameters by using different spectroscopic indicators as we describe in detail below. In our analysis, every time any of the parameters $T_{\rm eff}$, $\log g$, $\upsilon_{\rm mic}$, or abundances changed during the iteration process, we recalculated a new model by implementating the last measured quantities. The same concerns newly derived abundances: while the results of the abundance analysis depend upon the assumed model atmosphere, the atmospheric temperature-pressure structure itself depends upon the adopted abundances; we therefore recalculated the model atmosphere every time that the abundances were changed, even if the other model parameters were kept fixed. This procedure ensured that the model structure was consistent with the assumed abundances.

[1] http://www.eso.org/sci/facilities/lasilla/instruments/harps/tools/software.html

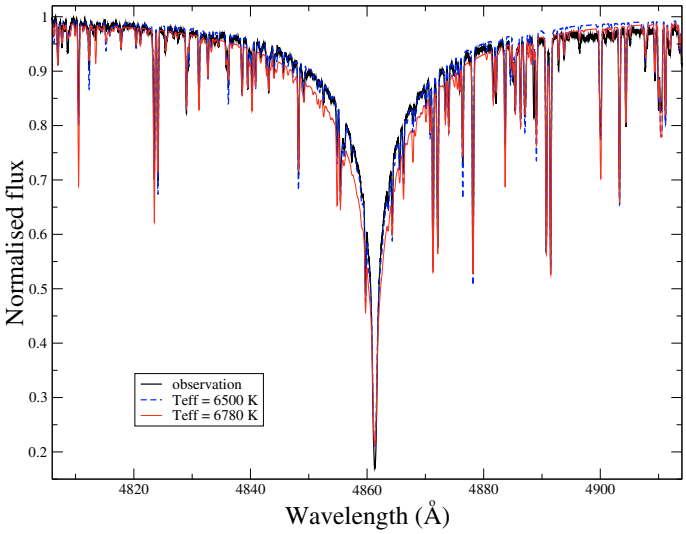

Fig. 1. Comparison between the observed Hβ line profile (solid line) and synthetic profiles calculated with the final adopted $T_{\rm eff} = 6500$ K (dashed line) and with $T_{\rm eff} = 6780$ K from Bruntt et al. (2008) (solid thin line). The dashed line agrees almost perfectly with the observed spectrum.

We performed the $T_{\rm eff}$ determination by fitting synthetic line profiles, calculated with SYNTH3 (Kochukhov 2007), to the observed profiles of three hydrogen lines: Hα, Hβ and Hγ. In the temperature range expected for HD 49933, hydrogen lines are extremely sensitive to temperature variations and very little to $\log g$ variations, and are therefore good temperature indicators. The $T_{\rm eff}$ obtained with this procedure is $T_{\rm eff} = 6500 \pm 50$ K. Figure 1 shows the comparison between the observed Hβ line profile and the synthetic profiles calculated with the adopted stellar parameters, as well as the synthetic profile obtained with the higher $T_{\rm eff} = 6780 \pm 130$ K published by Bruntt et al. (2008).

Another spectroscopic indicator for $T_{\rm eff}$ is given by the analysis of metallic lines. In particular, $T_{\rm eff}$ is determined by eliminating the correlation between line abundance and line excitation potential ($\chi_{\rm excit}$) for a given ion/element. This procedure can lead to erroneous parameters, so we decided not to take this indicator into account in our analysis. We discuss in Sect. 5 this important point extensively.

The surface gravity was derived from two independent methods based on line-profile fitting of Mg I lines with developed wings and the ionisation balance of several elements. Described in Fuhrmann et al. (1997), the first method assumes that the wings of the Mg I lines at $\lambda\lambda$ 5167, 5172, and 5183 Å are very sensitive to $\log g$ variations. In practice, we derived first the Mg abundance from other Mg I lines without developed wings, such as $\lambda\lambda$4571, 4730, 5528, and 5711 Å, and we then fit the wings of the other three lines by tuning the $\log g$ value. To apply this method, it is necessary to obtain very accurate $\log gf$ values and Van der Waals ($\log \gamma_{\rm Waals}$) damping constants for all the lines. The $\log gf$ values of the Mg lines given in the VALD database are of rather high quality and originate in laboratory measurements of the lifetimes (Anderson et al. 1967). However, new laboratory measurements of the oscillator strengths for Mg I lines at $\lambda\lambda$ 5167, 5172, and 5183 Å with an accuracy $\sigma \log gf = \pm 0.04$ dex were published by Aldenius et al. (2007). Van der Waals damping constants in VALD were calculated by Barklem & O'Mara (2000) but they appear to be slightly higher than needed to fit the solar lines. While $\log \gamma_{\rm Waals} = -7.27$ in Barklem & O'Mara (2000), Fuhrmann et al. (1997) derived

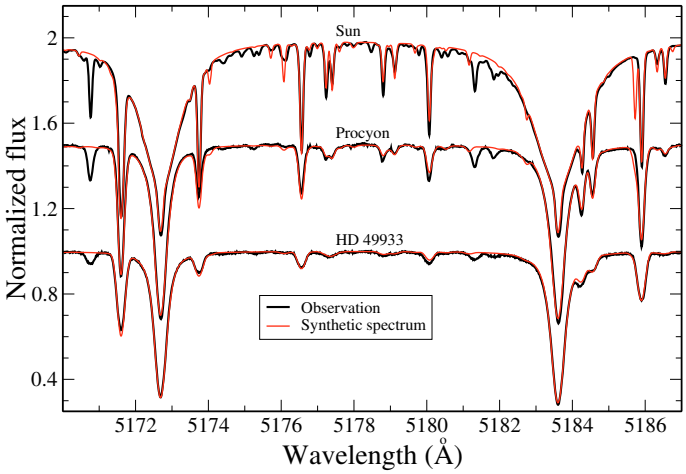

Fig. 2. Comparison between the observed Mg I line profiles used to determine $\log g$ (thick line) and synthetic profiles for the Sun, Procyon, and HD 49933, from top to bottom. The synthetic spectrum shown for HD 49933 was calculated with the final adopted $\log g = 4.00$ (thin line). For all three stars, we adopted the same combination of $\log gf$ and Van der Waals damping constants: oscillator strengths from Aldenius et al. (2007) and damping constants from Fuhrmann et al. (1997). See text for details on the observed spectra and adopted model atmospheres for the Sun and Procyon. The spectra of the Sun and Procyon were shifted upwards by 1 and 0.5, respectively.

$\log \gamma_{\rm Waals} = -7.42$ from the fitting of the solar lines using the Anderson et al. (1967) oscillator strengths. For our analysis, we employed different combinations of oscillator strengths and damping constants. Adopting oscillator strengths from Aldenius et al. (2007) and damping constants from Barklem & O'Mara (2000) or oscillator strengths from Anderson et al. (1967) and damping constants from Fuhrmann et al. (1997) we derived a $\log g$ value of 3.85, while adopting oscillator strengths from Aldenius et al. (2007) and damping constants from Fuhrmann et al. (1997) we obtained a $\log g$ value of 4.00. We obtained a formal $\log g$ value of 3.93 ± 0.07, where the given error bar on $\log g$ depends mainly on the uncertainty in the damping constant ($\gamma_{\rm Waals}$). Comparison of the synthetic colours with the observed ones (see Sect. 5.2) favors a $\log g$ value of 4.00 ± 0.15. Figure 2 shows a comparison between the synthetic and observed Mg I line profile for the 5172 and 5183 Å Mg I lines. The same procedure applied to the solar flux spectrum (Kurucz et al. 1984) resulted in $\log g = 4.44$ (oscillator strengths from Aldenius et al. 2007 and damping constants from Fuhrmann et al. 1997) and $\log g = 4.30$ for the combination of the oscillator strengths from Aldenius et al. (2007) and damping constants from Barklem & O'Mara (2000). The comparison of the observed and the synthetic Mg I line profile for the 5172 and 5183 Å Mg I lines for the Sun is shown in Fig. 2.

For surface gravity determination, one often uses ionisation equilibrium, but this method is extremely sensitive to the non-LTE effects present for each ion/element, while Mg lines with developed wings (less sensitive to non-LTE effects) are more suitable as $\log g$ indicators (Zhao & Gehren 2000). For this reason, we decided to retain Mg lines as our primary $\log g$ indicator checking afterwards the obtained result with the ionisation equilibrium. The $\log g$ value that we obtained ($\log g = 4.00 \pm 0.15$) is lower than that given by photometry and by other authors, e.g., Gillon & Magain (2006): $\log g = 4.26 \pm 0.08$ and Bruntt et al. (2008): $\log g = 4.24 \pm 0.13$. The difference between our result and, for example, those of both Gillon & Magain (2006) and Bruntt et al. (2008) is clearly connected with the difference in the derived effective temperature, while there is reasonable agreement for $\log g$, although the error bars are unfortunately quite large. This important point will be discussed in Sect. 5.

Since HD 49933 does not have an effective temperature high enough to show He lines, we are unable to measure the atmospheric He abundance. Diffusion calculations for low-mass metal poor stars show that helium should be depleted in the atmospheric layers (Proffitt & Michaud 1991), and therefore we tested the effect of a helium underabundance on the obtained parameters. We rederived $T_{\rm eff}$ and $\log g$ with hydrogen lines and Mg I line profiles respectively assuming a helium abundance of –2.0 dex and of –4.0 dex. In both cases, we measured no visible change in the hydrogen line profiles indicating no effect on the $T_{\rm eff}$ determination, while $\log g$ would have to be increased by about 0.15 for both helium underabundances, to be able to reproduce the Mg I line profiles adopted to derive $\log g$. This value is within the adopted uncertainty for $\log g$.

Our main source for the atomic parameters of spectral lines is the VALD database. LTE abundance analysis was based on equivalent widths, analysed with a modified version (Tsymbal 1996) of the WIDTH9 code (Kurucz 1993a). Although 301 Fe I lines were measured, only 158 lines with accurate experimental oscillator strengths were chosen for abundance determination to achieve the highest accuracy. First, we reject the lines with theoretical oscillator strengths. The rest of the lines were checked in the solar flux spectrum (Kurucz et al. 1984), observed with a resolving power $R \simeq 340\,000$ at wavelengths between 4000 Å and 4700 Å and with $R = 520\,000$ at longer wavelengths. The final choice was made for the lines that did not require an oscillator strength correction greater than 0.1 dex to fit the line cores of the solar spectrum. We also tried to have a set of Fe I lines uniformly distributed over the range of equivalent widths and excitation potentials. As for the lines of other elements/ions, we used nearly all unblended spectral lines with accurate atomic parameters available in the wavelength range 3850–6880 Å, except lines in spectral regions where the continuum normalisation was too uncertain. In case of blended lines, for lines affected by hyperfine splitting (*hfs*) or for lines situated in the wings of the hydrogen lines we derived the line abundance by performing synthetic spectrum calculations with the SYNTH3 code. The *hfs* constants for abundance calculations were taken from Blackwell-Whitehead et al. (2005) for Mn I lines, from Biehl (1976) for Ba II λ 4554 Å line and from Lawler et al. (2001) for Eu II lines. The effects of *hfs* are negligible for the two Cu I lines that we used in the abundance analysis.

The projected rotational velocity and macroturbulence ($\upsilon_{\rm macro}$) were determined by fitting synthetic spectra of several carefully selected lines in the observed spectrum. We obtained $\upsilon \sin i = 10 \pm 0.5$ km s^{-1} and $\upsilon_{\rm macro} = 5.2 \pm 0.5$ km s^{-1}. The value derived for $\upsilon_{\rm macro}$ agrees with that expected according to the relation $T_{\rm eff} - \upsilon_{\rm macro}$ published by Valenti & Fisher (2005) and obtained for a sample of more than a thousand stars.

Mosser et al. (2005) detected a line profile distortion that was variable with time of less than 500 m s^{-1}amplitude, probably due to granulation. This distortion is too small to be able to affect the parameter and abundance determination since the parameters were derived mainly with hydrogen and Mg I line profiles, while abundances were inferred from equivalent widths. The distortion of the line profiles could have, at most, increased the microturbulence velocity. It is known that Am stars also show distorted line profiles that increase in $\upsilon_{\rm mic}$ by 1.5–2.0 km s^{-1}, but for Am stars the distortion is of the order of 3–4 km s^{-1} (Landstreet 1998). If

Table 1. LTE atmospheric abundances HD 49933 with error estimates based on the internal scatter from the number of analysed lines, *n*.

Ion	HD 49933 – this paper				Bruntt et al. (2008)	Sun
	$\log(N/N_{\rm tot})$	n	$[N_{\rm el}/N_{\rm H}]_{\rm AGS}$	$[N_{\rm el}/N_{\rm H}]_{\rm GS}$	$[N_{\rm el}/N_{\rm H}]_{\rm GS}$	$\log(N/N_{\rm tot})$
C I	−3.74 ± 0.10	6	−0.09	−0.22	−0.56	−3.65
O I	−3.55	1	−0.17	−0.34	−0.53	−3.38
Na I	−6.15 ± 0.05	5	−0.28	−0.44	−0.36	−5.87
Mg I	−4.83 ± 0.07	4	−0.32	−0.37		−4.51
Mg II	−4.73	1	−0.22	−0.27		−4.51
Al I	−6.20:	2	−0.53	−0.63		−5.67
Si I	−4.86 ± 0.21	20	−0.33	−0.37	−0.37	−4.53
Si II	−4.82 ± 0.02	6	−0.29	−0.33		−4.53
S I	−5.23 ± 0.07	2	−0.33	−0.52	−0.36	−4.90
Ca I	−6.01 ± 0.11	26	−0.28	−0.33	−0.50	−5.73
Ca II	−6.01 ± 0.09	9	−0.28	−0.33		−5.73
Sc II	−9.24 ± 0.12	12	−0.25	−0.37	−0.45	−8.99
Ti I	−7.54 ± 0.07	19	−0.40	−0.52	−0.52	−7.14
Ti II	−7.42 ± 0.12	33	−0.28	−0.40	−0.41	−7.14
V I	−8.50 ± 0.13	4	−0.46	−0.46		−8.04
V II	−8.47 ± 0.23	5	−0.43	−0.43		−8.04
Cr I	−6.82 ± 0.17	25	−0.42	−0.45	−0.63	−6.40
Cr II	−6.61 ± 0.17	16	−0.21	−0.24	−0.43	−6.40
Mn I	−7.33 ± 0.14	14	−0.68	−0.68		−6.65
Fe I	−5.04 ± 0.06	158	−0.45	−0.50	−0.44	−4.59
Fe II	−5.03 ± 0.08	31	−0.44	−0.49	−0.44	−4.59
Co I	−7.49 ± 0.10	3	−0.37	−0.37		−7.12
Ni I	−6.34 ± 0.10	41	−0.53	−0.55	−0.48	−5.81
Cu I	−8.65 ± 0.07	2	−0.82	−0.82		−7.83
Zn I	−8.12±0.06	2	−0.66	−0.66		−7.44
Sr I	−9.65	1	−0.53	−0.58		−9.12
Sr II	−9.50 ± 0.04	3	−0.38	−0.43		−9.12
Y II	−10.34 ± 0.10	5	−0.51	−0.54		−9.83
Zr II	−9.85 ± 0.06	5	−0.40	−0.41		−9.45
Ba II	−10.06 ± 0.19	5	−0.19	−0.15		−9.87
La II	−11.21 ± 0.11	5	−0.30	−0.34		−10.91
Ce II	−10.73 ± 0.10	5	−0.27	−0.27		−10.46
Nd II	−10.77 ± 0.28	8	−0.18	−0.23		−10.59
Sm II	−11.09 ± 0.16	3	−0.06	−0.06		−11.03
Eu II	−11.92 ± 0.10	2	−0.40	−0.39		−11.52
Gd II	−11.16 ± 0.09	4	−0.24	−0.24		−10.92
Dy II	−11.36 ± 0.15	2	−0.46	−0.46		−10.90
$T_{\rm eff}$	6500 K				6780 K	5777 K
$\log g$	4.00				4.24	4.44

Fourth and fifth columns give HD 49933 abundances relative to the solar values from Asplund et al. (2005) (AGS) and from Grevesse & Sauval (1998) (GS), respectively. The sixth column gives abundances derived by Bruntt et al. (2008) relative to GS. The last column gives the abundances of the solar atmosphere from Asplund et al. (2005).

granulation played a role in increasing the derived value of $\upsilon_{\rm mic}$, it is probably less than 0.1 km s^{-1}, which is below our detection limit.

The microturbulence was determined by minimising the correlation between equivalent width and abundance for several ions. We used mainly Fe I lines since this is the ion that provides the largest number of measured lines within a wide range of equivalent width, but the correlations obtained with Ti I, Ti II, Cr I, Fe II, and Ni I lines were also taken into account. The microturbulent velocities have values between 1.4 km s^{-1} (Ti I) and 1.9 km s^{-1} (Ti II) with an average of $\upsilon_{\rm mic}$ = 1.60 ± 0.18 km s^{-1}. The microturbulent velocity derived from Fe I lines is 1.5 km s^{-1}. This value, which has an uncertainty of 0.2 km s^{-1}, was adopted for the final analysis as that providing the most accurate representation of all lines of neutral elements. Figure 5 (online material) displays the correlation between the line abundance of Fe I and the measured equivalent widths.

The final abundances are given in Table 1. We also computed the abundance difference between HD 49933 and the solar atmosphere as derived by Asplund et al. (2005) (4th Col.) and by Grevesse & Sauval (1998) (5th Col). The results of the abundance analysis of HD 49933 taken from Bruntt et al. (2008) are given in the 6th column of Table 1 for comparison.

The stellar metallicity (Z) is defined as follows:

$$Z_{\rm star} = \frac{\sum_{a\geq 3} m_a 10^{\log(N_a/N_{\rm tot})}}{\sum_{a\geq 1} m_a 10^{\log(N_a/N_{\rm tot})}}, \quad (1)$$

where a is the atomic number of an element with atomic mass m_a. Making use of the abundances obtained from the performed analysis, we derived a metallicity of Z = 0.008 ± 0.002 dex, adopting the solar abundances by Asplund et al. (2005) for all the elements that were not analysed. However, if we assume an underabundance of −0.5 dex for *all* elements not been analysed the resulting Z value remains practically unchanged. Scaling the solar abundances of all elements by −0.5 dex gives the metallicity Z = 0.006 dex. This substantial difference in Z illustrates that it is important to derive an accurate determination of C and O, which provides a large contribution to the determination of Z.

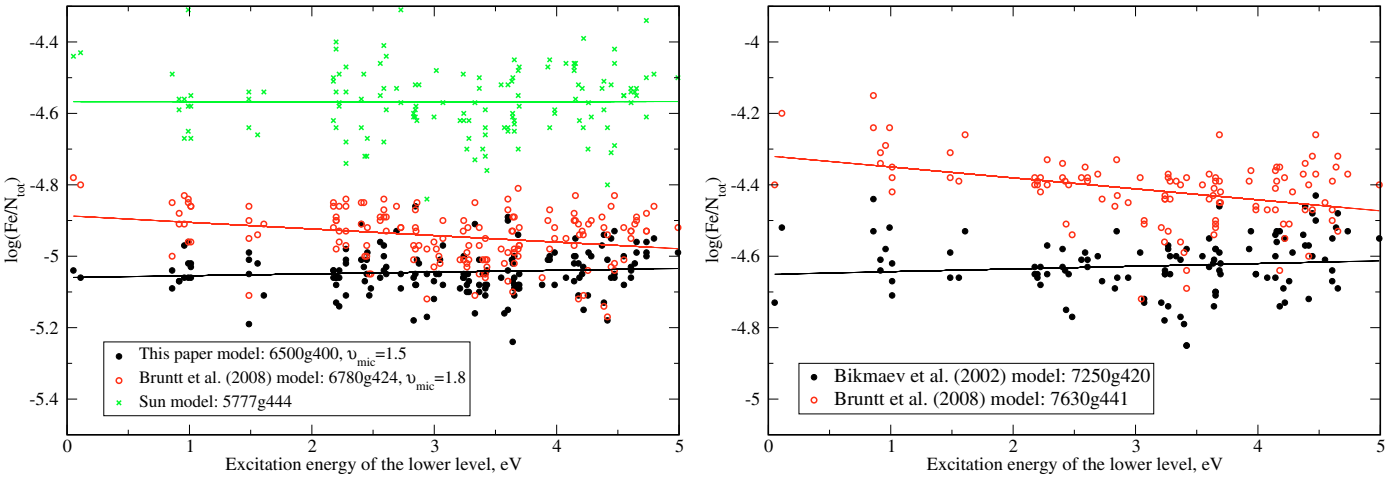

Fig. 3. Plots of individual abundances for 158 Fe I Lines versus the excitation energy of the lower level for HD 49933 (*left panel*) and HD 32115 (*right panel*) with different model atmospheres. The same dependence for 137 common Fe lines in the solar spectrum is shown by crosses in the left panel.

Additionally, a He underabundance of −1 and −3 dex relative to Sun does not change the Z value.

4.1. Abundance uncertainties

The abundance uncertainties shown in Table 1 are the standard deviation of the mean abundance from the individual line abundances and do not represent the true error bars associated with each of the derived element abundances.

Based on realistic errors on the equivalent width measurements, we found that the uncertainty in the abundance of a given line is only about 0.01 dex (see Fossati et al. 2009, for more details). In the case of ions with a sufficiently high number of lines, we assume that the internal scatter for each ion includes the uncertainties due to both equivalent width measurement and continuum normalisation.

Plotting the abundance scatter as a function of the number of lines, it is possible to determine that the mean scatter applicable when only one line of a certain ion is measured. In these cases, it is reasonable to assume an internal error of 0.10 dex.

The internal scatter is just part of the total abundance error bar since the uncertainties in the fundamental parameters also play an important role. Table 3 (online material) shows the variation in abundance caused by changing each parameter ($T_{\rm eff}$, $\log g$, and $\upsilon_{\rm mic}$) by $+1\sigma$ and the final adopted uncertainty for each ion following the standard error analysis. The main source of uncertainty is the effective temperature, while the uncertainties related to $\log g$ and in particular to $\upsilon_{\rm mic}$ are almost negligible. Assuming that the contributions to the uncertainty in the abundances are independent, we derive the final uncertainty using error propagation. The result is given in Col. 7 of Table 3 (available as online material).

5. Discussion

Our abundance calculation using different atmospheric models proposed in the literature shows that the accuracy (rms) of the abundance determination is the same for practically all of them and any difference in absolute value is caused by differences in the model parameters. Therefore, we compare and discuss the determination of the atmospheric parameters.

5.1. Comparison with previous determinations

The published effective temperatures of HD 49933 range from 6300 K (Hartmann & Gehren 1988) 6484 K (Blackwell & Lynas-Gray 1998) (IR flux method), and 6595 K (Edvardsson et al. 1993) (Strömgren photometry) to 6735–6780 K (Gillon & Magain 2006; Bruntt et al. 2004, 2008). The last three cited works employed the spectrum synthesis iterative methods of APASS and VWA. For more details about previously derived atmospheric parameters, the reader is also referred to Table 4 of Bruntt et al. (2004). The APASS and VWA methods used the correlation of the abundance of neutral Fe lines with an excitation potential as an indicator of $T_{\rm eff}$. The final $T_{\rm eff}$ is found by minimising this correlation. Hydrogen lines are not considered in the APASS and VWA methods. It is important to emphasise that in the APASS method (Gillon & Magain 2006) the continuum level is adjusted in each iteration. Gillon & Magain (2006) also obtained very different temperature estimates working with both APASS ($T_{\rm eff} = 6735 \pm 53$ K) and equivalent widths ($T_{\rm eff} = 6538 \pm 44$ K). The authors favored the APASS results because the Gaussian approximation of the line profiles (used to measure equivalent widths) in a spectrum of a star rotating with $\upsilon \sin i = 10$ km s^{-1} overestimates the equivalent widths. Since we used equivalent widths, we investigated this possible error source by calculating synthetic profiles of 26 Fe I lines in the range 6–122 mÅ with our adopted model atmosphere and for an Fe abundance of $\log({\rm Fe}/N_{\rm tot}) = -5.05$. We measured their equivalent widths with direct integration, broadened the synthetic spectrum with the instrumental, rotational and macroturbulent velocity profiles, and then again measured equivalent widths by Gaussian approximation of the convolved spectrum. Inserting both sets of equivalent widths in the WIDTH9 code we derived an average abundance of $\log({\rm Fe}/N_{\rm tot}) = -5.050 \pm 0.004$ adopting directly integrated equivalent widths and of $\log({\rm Fe}/N_{\rm tot}) = -5.040 \pm 0.016$ adopting the Gaussian approximation, as shown in Table 4 in the Online material. No significant indications of change in microturbulent velocity or effective temperature appeared in the second case. Thus we, conclude that in HD 49933 the use of equivalent widths instead of synthetic spectrum should not influence the determination of the model parameters.

The use of both the APASS and the VWA (Bruntt et al. 2008) methods also leads to a higher $T_{\rm eff}$ for HD 49933 and another star HD 32115, for which the effective temperature

was derived by Bikmaev et al. (2002) with the same method (Strömgren photometry and hydrogen line profiles) as in the present paper. Figure 3 shows individual abundances from 158 Fe I lines calculated with the model parameters derived in this paper ($T_{\rm eff}$ = 6500 K, $\log g$ = 4.00) and by Bruntt et al. (2008) ($T_{\rm eff}$ = 6780 K, $\log g$ = 4.24) versus the excitation energy of the lower level. For both models, the microturbulent velocity, derived by us in the usual way, is nearly the same, 1.5 km s^{-1} and 1.6 km s^{-1}, respectively. However, to be consistent with the results by Bruntt et al. (2008) we plot abundances versus excitation potential for Bruntt's model using $\upsilon_{\rm mic}$ = 1.8 km s^{-1} derived in Bruntt et al. (2008). The same dependence was also calculated for HD 32115 using equivalent width measurements from Bikmaev et al. (2002) and model atmospheres from Bikmaev et al. (2002) and from Bruntt et al. (2008). As a final check, we used the solar flux spectrum. We analysed 137 out of 158 Fe I lines with the solar model atmosphere ($T_{\rm eff}$ = 5777 K, $\log g$ = 4.44) also calculated with the LLMODELS code. There were 21 discarded lines that could not be properly fitted in the solar spectrum. Seven lines are blended in the Sun, which is cooler and more metallic than HD 49933, while the remaining 14 lines have extended wings and cannot be accurately measured. Our analysis inferred in $\log({\rm Fe}/N_{\rm tot}) = -4.57 \pm 0.09$ for $\upsilon_{\rm mic}$ = 0.95 km s^{-1} in full agreement with the currently adopted solar parameters (Asplund et al. 2005). Individual abundances derived from the solar Fe I lines versus the excitation energy of the lower level are shown in Fig. 3.

In Fig. 3, one immediately notices the negative slope, indicating too high value of a $T_{\rm eff}$, adopting the model parameters obtained by Bruntt et al. (2008) for both stars. This and the poor fit to the hydrogen line profiles (see Fig. 1) clearly shows that both automatic methods based on synthetic spectrum calculations, ignoring hydrogen lines, lead to an overestimate of the effective temperature by ~200 K. With our model, we derive a small positive slope that formally corresponds to an underestimate of the $T_{\rm eff}$ by ~30 K. For the Sun, a zero slope is obtained.

Our temperature is close to that derived with the IR flux method by Blackwell & Lynas-Gray (1998), $T_{\rm eff} = 6484 \pm 45$ K, and provides a good description of all global observables: photometric colours, hydrogen, and metallic line profiles.

Our value for the surface gravity is supported by the ionisation equilibrium for Fe I/Fe II and few other elements, such as Si I/Si II and Ca I/Ca II. Even for Ti and Cr, for which we have enough lines for an accurate abundance analysis, the average abundances from the two ionisation stages agree within the error bars. Applying a higher microturbulence of 1.9 km s^{-1}, derived from Ti II lines, for example, leads to a Ti I/Ti II equilibrium. In the case of chromium, about half of the analysed Cr II lines and one third of Cr I lines have theoretically calculated oscillator strengths, which may influence the final abundance results. The atmospheric parameters derived for HD 49933 are similar to those of another solar-type pulsator, Procyon, which has $T_{\rm eff} = 6512 \pm 49$ K, $\log g = 3.96 \pm 0.02$, and $\log({\rm Fe}/N_{\rm tot}) = -4.60 \pm 0.15$ (Allende Prieto et al. 2002). The comparison of the observed and synthetic Mg I line profile for the 5172 and 5183 Å Mg I lines for Procyon is shown in Fig. 2 (see Ryabchikova et al. 2008, for details about the observed spectrum of Procyon and the adopted model atmosphere).

5.2. Synthetic photometry

Since there are no available observations of HD 49933 in the visible spectral region, calibrated to physical units, we adopted photometric observations extracted from the SIMBAD database[2]. Table 2 summarises the comparison between observed and theoretical colour-indices of different photometric systems. The theoretical colours were computed using computer codes by Kurucz (1993a) modified to read and process high-resolution fluxes produced by the LLMODELS. The reddening, corresponding to $E(B-V) = 0$, was derived using analytical extinction models by Amôres & Lépine (2005). Besides the final model with $T_{\rm eff}$ = 6500 K, $\log g$ = 4.0 (Model 1), we also present the synthetic photometry for three other models: $T_{\rm eff}$ = 6500 K, $\log g$ = 3.85 (Model 2); a model with the parameters derived from the Strömgren photometry ($T_{\rm eff}$ = 6550 K, $\log g$ = 4.25, Model 3); and a model with the parameters published by Bruntt et al. (2008) ($T_{\rm eff}$ = 6780 K, $\log g$ = 4.24, Model 4).

Table 2. Observed and calculated photometric parameters of HD 49933.

Colour index	**SIMBAD**	t6500g4.0 (Model 1)	t6500g3.85 (Model 2)	t6550g4.25 (Model 3)	t6780g4.24 (Model 4)
$b-y$	**0.270** (0.002)	0.2754	0.2727	0.2724	0.2399
m_1	**0.127** (0.004)	0.1251	0.1255	0.1330	0.1355
c_1	**0.460** (0.003)	0.5123	0.5502	0.4400	0.5126
$H\beta$	**2.662**	2.7272	2.7291	2.7279	2.7501
$B-V$	**0.390**	0.3865	0.3829	0.3865	0.3371
$U-B$	**−0.070**	−0.0628	−0.0457	−0.0942	−0.0882
Geneva					
$U-B$	**1.235**	1.2561	1.2896	1.1950	1.2285
$V-B$	**0.491**	0.5125	0.5166	0.5123	0.5700
B_1-B	**0.973**	0.9842	0.9835	0.9878	0.9723
B_2-B	**1.391**	1.4142	1.4152	1.4102	1.4252
V_1-B	**1.224**	1.2423	1.2461	1.2420	1.2962
$G-B$	**1.586**	1.6135	1.6185	1.6146	1.6847

The values in brackets give the error bars of observations.

It is seen from the Table 2 that the Strömgren and UBV indices are described more accurately by Model 1. The Hβ index shows a poor fit to all models, but this does not play a critical role in the present study since the profiles of hydrogen lines were reproduced perfectly with the parameters of Model 1. The colour-indices of the Geneva system are generally described more accurately by Model 1, 2 and 3, i.e., models with lower $T_{\rm eff}$. However, the indices $U-B$ and B_1-B are better fitted with a higher temperature (Model 4). Model 1 and 3 show a comparable fit, with the difference that Model 1 reproduces the $\log g$ sensitive $c1$ index more effectively, but less effectively reproduces the $U-B$ index, while for Model 3 it is the opposite. In summary, we find that the majority of the photometric indicators and the present accurate spectroscopic study point to the adopted $T_{\rm eff}$ = 6500 K and $\log g$ = 4.0.

6. Conclusions

Based on ten high-resolution, high signal-to-noise spectra taken from ESO archive, we carried out a precise spectroscopic analysis of one of the primary solar-like CoRoT targets HD 49933. All ten spectra were averaged to obtain a single spectrum with a resolution $R \approx 115\,000$ and signal-to-noise ratio ≈500 per pixel at $\lambda \approx 5000$ Å. Using this spectrum, we revised the fundamental parameters and the atmospheric abundances in a

[2] http://simbad.u-strasbg.fr/simbad/

consistent way employing modern 1D LTE stellar model atmospheres (LLmodels; Shulyak et al. 2004). The derived set of fundamental parameters and abundances provide a good fit to the available observables: IR and multicolour photometry, pressure-sensitive magnesium lines, metallic lines, and profiles of hydrogen Balmer lines.

It is shown that the implementation of automatic procedures for the abundance analysis using only line spectra without hydrogen lines can result in inaccurate parameters and hence abundances.

Acknowledgements. This work was supported by following funding projects: FWF Lise Meitner grant Nr. M998-N16 (DS), by the Presidium RAS Programme "Origin and evolution of stars and galaxies", and by the Leading Scientific School grant 4354.2008.2 (TR). L.F. has received support from the Austrian Science Foundation (FWF project P19962 – Modulated RR Lyrae Stars). We kindly thank Thomas Kallinger and Michael Gruberbauer for the useful discussions and comments during the preparation of the draft.

References

Aldenius, M., Tanner, J. D., Johansson, S., Lundberg, H., & Ryan, S. G. 2007, A&A, 461, 767
Allende Prieto, C., Asplund, M., Garćia Lopez, R. J., & Lambert, D. 2002, ApJ, 567, 544
Amôres, E. B., & Lépine, J. R. 2005, AJ, 130, 659
Anderson, E. M., Zilitis, V. A., & Sorokina, E. S. 1967, Opt. Spectr., 23, 102
Appourchaux, T., Michel, E., Auvergne, M., et al. 2008, A&A, 488, 705
Asplund, M., Grevesse, N., & Sauval, A. J. 2005, ASP Conf. Ser., 336, 25
Barklem, P. S., & O'Mara, B. J. 2002, MNRAS, 311, 535
Bikmaev, I. F., Ryabchikova, T. A., Bruntt, H., et al. 2002, A&A, 389, 537
Biehl, D. 1976, Ph.D. Thesis, Christian-Albrechts-Universität, Kiel, Institute für Theoretische
Blackwell, D. E., & Lynas-Gray, A. E. 1998, A&AS, 129, 505
Blackwell-Whitehead, R. J., Pickering, J. C., & Pearse, O. 2005, ApJS, 157, 402
Bruntt, H., Bikmaev, I. F., Catala, C., et al. 2004, A&A, 425, 683
Bruntt, H., De Cat, P., & Aerts, C. 2008, A&A, 478, 487
Burleigh, M. R., Barstow, M. A., & Fleming, T. A. 1997, MNRAS, 287, 381
Canuto, V. M., & Mazzitelli, I. 1991, ApJ, 370, 295
Canuto, V. M., & Mazzitelli, I. 1992, ApJ, 389, 724
Cenarro, A. J., Peletier, R. F., Sánchez-Blázquez, P., et al. 2007, MNRAS, 374, 664
Edvardsson, B., Andersen, J., Gustafsson, B., et al. 1993, A&A, 275, 101
Fossati, L., Ryabchikova, T., Bagnulo, S., et al. 2009, A&A, 503, 945
Fuhrmann, K., Pfeiffer, M., Frank, C., Reetz, J., & Gehren, T. 1997, A&A, 323, 909
Gillon, M., & Magain, P. 2006, A&A, 448, 341
Grevesse, N., & Sauval, A. J. 1996, ASP Conf. Ser., 99, 117
Gruberbauer, M., Kallinger, T., Weiss, W. W., & Guenther, D. B. 2008, A&A, in press [arXiv:0811.3345]
Guenther, D. B., Demarque, P., Kim, Y.-C., & Pinsonneault, M. H. 1992, ApJ, 387, 372
Hartmann, K., & Gehren, T. 1988, A&A, 199, 269
Heiter, U., Kupka, F., van't Veer-Menneret, C., et al. 2002, A&A, 392, 619
Kallinger, T., Gruberbauer, M., Guenther, D. B., Fossati, L., & Weiss, W. W. 2008, A&A, submitted [arXiv:0811.4686]
Kochukhov, O. 2007, Spectrum synthesis for magnetic, chemically stratified stellar atmospheres, Physics of Magnetic Stars, 109, 118
Kupka, F., Piskunov, N., Ryabchikova, T. A., Stempels, H. C., & Weiss, W. W. 1999, A&AS, 138, 119
Kurucz, R. 1993, ATLAS9: Stellar Atmosphere Programs and 2 km s^{-1} grid. Kurucz CD-ROM No. 13 (Cambridge: Smithsonian Astrophysical Observatory)
Kurucz, R. L., Furenlid, I., Brault, J., & Testerman, L. 1984, NSO Atlas No. 1: Solar Flux Atlas from 296 to 1300 nm, Sunspot, NSO
Landstreet, J. D. 1998, A&A, 338, 1041
Lawler, J. E., Wickliffe, M. E., Den Hartog, E. A., & Sneden, C. 2001b, ApJ, 563, 1075
Marigo, P., Girardi, L., Bressan, A., et al. 2008, A&A, 482, 883
Mosser, B., Bouchy, F., Catala, C., et al. 2005, A&A, 431, L13
Pietrinferni, A., Cassisi, S., Salaris, M., & Castelli, F. 2004, ApJ, 612, 168
Piskunov, N. E., Kupka, F., Ryabchikova, T. A., Weiss, W. W., & Jeffery, C. S. 1995, A&AS, 112, 525
Proffitt, C. R., & Michaud, G. 1991, ApJ, 371, 584
Przybilla, N., Butler, K., Becker, S. R., & Kudritzki, R. P. 2006, A&A, 445, 1099
Rogers, N. Y. 1995, Comm. Astroseismol., 78
Ryabchikova, T. A., Piskunov, N. E., Stempels, H. C., Kupka, F., & Weiss, W. W. 1999, Phis. Scr., T83, 162
Ryabchikova, T. A., Kochukhov, O., & Bagnulo, S. 2008, A&A, 480, 811
Shulyak, D., Tsymbal, V., Ryabchikova, T., Stütz Ch., & Weiss, W. W. 2004, A&A, 428, 993
Valenti, J. A., & Fisher, D. A. 2005, ApJS, 159, 141
Tsymbal, V. V. 1996, in Model Atmospheres and Spectral Synthesis, ed. S. J. Adelman, F. Kupka, & W. W. Weiss, ASP Conf. Ser. 108, 198
Zhao, G., & Gehren, T. 2000, A&A, 362, 1077

Pages 210 and 211 (Figs. 4, 5 and Tables 3, 4) are available in the electronic edition of the journal at http://www.aanda.org

Table 3. Error sources for the abundances of the chemical elements in HD 49933.

Ion	abundance $\log(N/N_{\rm tot})$	$\sigma_{\rm abn}$ (scatt.) (dex)	$\sigma_{\rm abn}$ ($T_{\rm eff}$) (dex)	$\sigma_{\rm abn}$ ($\log g$) (dex)	$\sigma_{\rm abn}$ ($\upsilon_{\rm mic}$) (dex)	$\sigma_{\rm abn}$ (tot) (dex)
C I	−3.74	0.10	−0.02	0.05	0.00	0.11
O I	−3.55		−0.03	0.05	0.00	0.12
Na I	−6.15	0.05	0.02	0.00	−0.01	0.05
Mg I	−4.83	0.07	0.03	−0.01	−0.02	0.08
Mg II	−4.73		−0.02	0.05	−0.01	0.11
Al I	−6.20		0.02	0.00	0.00	0.10
Si I	−4.86	0.21	0.01	0.00	−0.01	0.21
Si II	−4.82	0.02	−0.03	0.05	−0.02	0.07
S I	−5.23	0.07	−0.01	0.04	0.00	0.08
Ca I	−6.01	0.11	0.03	−0.01	−0.05	0.12
Ca II	−6.01	0.09	−0.02	0.05	−0.01	0.11
Sc II	−9.24	0.12	0.02	0.05	−0.05	0.14
Ti I	−7.54	0.07	0.03	0.00	−0.02	0.08
Ti II	−7.42	0.12	0.01	0.05	−0.05	0.16
V I	−8.50	0.13	0.04	0.00	−0.01	0.15
V II	−8.47	0.23	0.01	0.05	−0.01	0.15
Cr I	−6.82	0.17	0.04	0.00	−0.02	0.18
Cr II	−6.61	0.17	0.00	0.05	−0.03	0.19
Mn I	−7.33	0.14	0.03	0.00	−0.03	0.15
Fe I	−5.04	0.06	0.04	−0.01	−0.04	0.13
Fe II	−5.03	0.08	0.01	0.05	−0.05	0.12
Co I	−7.49	0.10	0.03	0.00	0.00	0.10
Ni I	−6.34	0.10	0.03	0.00	−0.02	0.11
Cu I	−8.65	0.07	0.03	0.00	−0.01	0.08
Zn I	−8.12	0.06	0.02	0.01	−0.04	0.08
Sr I	−9.65		0.03	0.00	0.00	0.10
Sr II	−9.50	0.04	0.01	0.06	−0.01	0.07
Y II	−10.34	0.10	0.02	0.05	−0.02	0.12
Zr II	−9.85	0.06	0.01	0.05	−0.01	0.08
Ba II	−10.06	0.19	0.03	0.02	−0.07	0.16
La II	−11.21	0.11	0.03	0.06	0.00	0.14
Ce II	−10.73	0.10	0.03	0.05	0.00	0.12
Nd II	−10.77	0.28	0.02	0.05	−0.01	0.28
Sm II	−11.09	0.16	0.03	0.05	0.00	0.17
Eu II	−11.92	0.10	0.03	0.05	0.00	0.12
Gd II	−11.16	0.09	0.03	0.05	0.00	0.15
Dy II	−11.36	0.15	0.03	0.05	0.00	0.16

Column 3 gives the standard deviation $\sigma_{\rm abn}$ (scatt.) of the mean abundance obtained from different spectral lines (internal scatter); a blank means that the number of spectral lines is <2, hence no internal scatter could be estimated. (Note that these values are identical to those given in Table 1). Columns 4–6 give the variation in abundance estimated by increasing $T_{\rm eff}$ by 50 K, $\log g$ by 0.15 dex, and $\upsilon_{\rm mic}$ by 0.2 km s^{-1}, respectively. Column 7 gives the the mean error calculated applying standard error propagation theory on the uncertainties given in the previous columns, i.e., $\sigma^2_{\rm abn}$ (tot) = $\sigma^2_{\rm abn}$ (scatt.) + $\sigma^2_{\rm abn}$ ($T_{\rm eff}$) + $\sigma^2_{\rm abn}$ ($\log g$) + $\sigma^2_{\rm abn}$ ($\upsilon_{\rm mic}$). For the computation of $\sigma^2_{\rm abn}$ (tot) of those ions for which the internal scatter could not be measured, we have assumed a priori $\sigma_{\rm abn}$ (scatt.) = 0.10 dex.

Table 4. Comparison between the line abundances obtained for a set of Fe I lines calculated from equivalent widths measured with direct integration and a Gaussian approximation.

	Direct integration		Gaussian measurements	
Wavelength	EqW	Abundance	EqW	Abundance
Å	mÅ		mÅ	
5123.7200	60.30	−5.05	61.31	−5.02
5127.3593	52.50	−5.05	53.41	−5.03
5133.6885	87.60	−5.06	87.23	−5.06
5139.4628	105.10	−5.05	104.48	−5.06
5141.7393	53.20	−5.05	54.11	−5.03
5142.9285	62.00	−5.05	63.03	−5.02
5162.2729	85.60	−5.05	84.42	−5.07
5165.4100	73.90	−5.05	74.55	−5.04
5171.5964	98.20	−5.05	99.20	−5.03
5184.2661	22.80	−5.05	23.24	−5.04
5191.4550	98.80	−5.05	98.57	−5.05
5192.3442	107.70	−5.05	106.98	−5.06
5194.9418	82.90	−5.05	84.00	−5.02
5602.9451	67.20	−5.05	68.04	−5.03
5615.2966	24.00	−5.05	24.30	−5.04
5615.6439	122.60	−5.06	120.95	−5.08
5618.6327	15.70	−5.05	16.10	−5.03
5620.4924	6.10	−5.05	6.24	−5.04
5624.0220	7.80	−5.04	7.74	−5.05
5624.5422	72.50	−5.05	73.44	−5.03
5631.7310	6.30	−5.04	6.39	−5.04
5633.9465	28.50	−5.05	29.03	−5.03
5638.2621	31.00	−5.05	31.58	−5.03
5640.3070	6.20	−5.05	6.33	−5.04
5641.4340	17.50	−5.05	17.88	−5.03
5655.4930	32.60	−5.05	33.20	−5.03
Mean ± rms		−5.050 ± 0.004		−5.040 ± 0.016

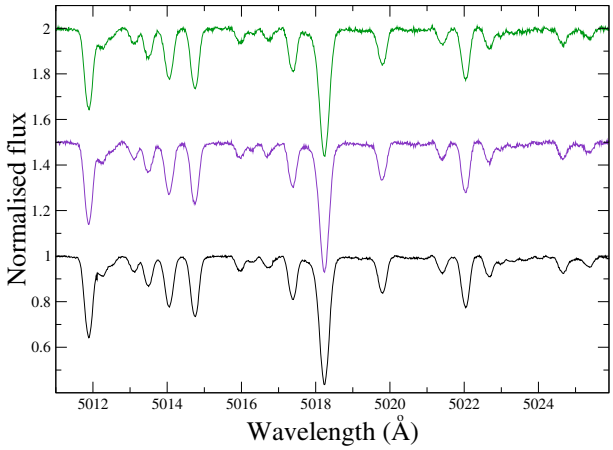

Fig. 4. Samples of the first spectrum obtained February 11th, the last obtained February 13th and the final co-added spectrum (from top to bottom) around the strong Fe II line at ~5018 Å.

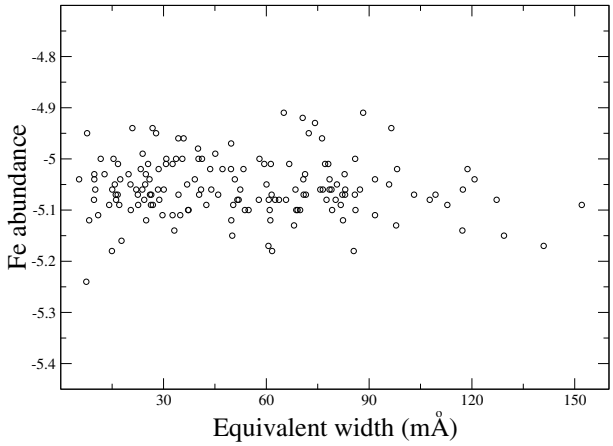

Fig. 5. ionFei individual line abundances vs. equivalent widths. Abundances are derived for the preferred model parameters, $T_{\rm eff}$ = 6500 K, $\log g$ = 4.00, $\upsilon_{\rm mic}$ = 1.5 km s^{-1}.